Tellus (1996), 48A, 290–311
Printed in Belgium – all rights reserved

TELLUS
ISSN 0280–6495

On the dynamical coupling of large-scale spatial patterns of rainfall and soil moisture

By FABIO CASTELLI*, *Istituto di Idraulica, Università degli Studi di Perugia, Loc. S. Lucia, 06125 Perugia, Italy*, and IGNACIO RODRIGUEZ-ITURBE, *Department of Civil Engineering, Texas A & M University, College Station, Texas 77843, USA*

(Manuscript received 13 July 1994; in final form 8 June 1995)

ABSTRACT

It is well-recognized, although not really well understood, the impact that land-atmosphere interaction has on the large variability in the spatial structure of continental climate. This paper focuses on a specific dynamical coupling between the soil moisture and atmospheric processes, such as in the presence of a growing moist baroclinic wave. Starting from the inviscid semi-geostrophic equations for the evolution of a meridionally independent baroclinic disturbance in the moist atmosphere, a discretized fluid-dynamical model is formulated. A quite general scheme for the representation of the mass and energy exchanges between the soil and the atmospheric boundary layer is also included, and analytical solutions to the non-linear instability problem are derived. The analysis of these solutions show how a heterogeneous soil moisture modifies the dynamics of the baroclinic wave up to the formation of atmospheric fronts, and how a rough estimate of the associated rainfall potential is affected as well. In particular, when the baroclinic wave develops in such a way that the warm precipitating anomaly develops on top of wet soil, with dry soil on the cold anomaly side, both the occurrence of the frontal collapse and the rainfall potential are favored. A positive, spatially structure, feedback of soil moisture on its own precipitation forcing is then identified.

1. Introduction

It is well-recognized, although not really well-understood, the impact that land-atmosphere interaction has on the continental climate. If land evapotranspiration partially feeds precipitating clouds, then the land hydrology may be said to exert influence on its own forcing. This basic non-linear character of the problem is responsible for the unexpected behavior of the system when subjected to random fluctuations. Rodriguez-Iturbe et al. (1991) and Entekhabi et al. (1992) have shown that hydrologic balance models which include precipitation recycling may yield bimodal climates where the system locks into a drought mode or a pluvial mode and persists there for several years.

This paper is a further step in the direction of studying the dynamic coupling of large scale spatial patterns of rainfall and soil moisture. Entekhabi and Rodriguez-Iturbe (1994) have approached this problem from a probabilistic perspective in which a stochastic rainfall field is imposed on the driven mechanism of a simple balance equation describing the soil moisture dynamics. The spectral and correlation properties of the soil moisture field are derived as a function of the input and the parameters existing in the balance equation. This approach does not include feedback between land and atmospheric processes and thus it will not allow the study of evolutionary patterns neither in soil moisture nor in atmospheric disturbances. The present paper attempts to build an explicitly coupled dynamics between the soil moisture and the atmosphere. The coupling occurs through mass (precipitation and evaporation) and energy exchanges (sensible and latent heat).

* Corresponding author.

The weather system at the mid latitudes is characterized by the continuous alternation, development and decay of movable cyclones and anti-cyclones, with typical temporal scales of a few days and spatial scales of a few thousand kilometers. Such synoptic structures are known, since Charney (1947) and Eady (1949), to be the result of the instability of the mean zonal flow with respect to small perturbations in the flow itself, commonly defined as baroclinic instability. This instability of the zonal flow is mainly due to the vertical shear which, in the undisturbed flow, is in geostrophic balance with the horizontal temperature gradient between polar and tropical regions (thermal wind).

Most of the precipitation at the mid latitudes is produced by such a phenomena, either directly, by the cyclonic large-scale convergence, or indirectly, by the induced frontogenesis. In particular, it is well known that the uplift forcing provided by frontal circulation, coupled with smaller scale instabilities such as the symmetric one (Seltzer et al., 1985), may lead to very complex precipitation patterns, with a large variety of spatio-temporal scales and intensities (Houze, 1981; Houze and Hobbs, 1982).

Some recent works, based on simulations of case-studies with primitive-equations numerical models, have addressed the possible effects of heterogeneous soil moisture distributions on large mesoscale circulation. In Chang and Wetzel (1991), the prestorm environment connected to the development of a convective complex in Nebraska on 3–4 June 1980 is analyzed by comparing different simulations based on different hypothesis on the soil moisture and vegetation distributions: spatial variations in both quantities are found to lead to the enhancement of a stationary front. With a similar approach, Fast and McCorcle (1991) analyze the passage of a summer cold front in the central United States. The evaporating heterogeneous soil is found to significantly alter the structure of the boundary layer embedded in the baroclinic circulation. As a result, the front is now weakened near the surface, with an increase of moisture convergence in several locations and the advection of the evaporated moisture far from the origin. Both studies recognizes the important role of soil moisture in modifying the spatial distribution and intensity of precipitation, still highlighting a strong dependence of these effects on the particular synoptic conditions.

Some other studies, such as by Ookouchi et al. (1984) and by Segal et al. (1988), had already indicated that the intensity of thermal circulation induced by soil heterogeneity may reach, even in the absence of significant synoptic forcing, that of the sea-breeze circulation.

Taking these results as "evidences" of significant effects of soil moisture on precipitation at a variety of scales, there is then a need for a deeper conceptual understanding of the underlying feedback mechanisms.

Our interest is in the investigation of possible mechanism leading to the long (months or years) persistence of climatic anomalies. To this respect, the precipitation dynamics produced by mid-latitude cyclonic perturbations may be seen as the occurrence of random events in time, having particular spatial structures. A long lasting anomaly in the soil moisture distribution may develop, provided that a feedback mechanism exists from the soil moisture itself on the precipitation dynamics. In particular, we may argue that a positive soil moisture anomaly is able to induce an increase in the rate of occurrence and in the average intensity of the precipitation events.

In other words, we may ask the question if there exist a preferred coupling between the alternation of warm-cold (cyclonic-anticyclonic) anomalies of a baroclinic wave and large-scale spatial patterns in the soil moisture distribution. By preferred we mean that given uniform (in a probabilistic sense) initial conditions in all the variables other than the soil moisture distribution, the coupling could lead to either a more probable birth of the baroclinic disturbance, a faster growth of the corresponding wave or, more important, a higher estimate of the precipitation produced in the cyclonic areas.

The effect of a "moist" surface boundary on the development of ideal baroclinic waves was studied, as an example, in Fantini (1991). Such a study was based on the two-level moist semigeostrophic model of Emanuel et al. (1987) (hereafter referred to as E87), with the addition of parametrized heat and moisture fluxes from a warm sea body. Even if in a qualitative way, given the simplified form of the model, and in the restriction of the "warm sea" case (evaporation always present at its potential rate), the study clarified some important mechanisms leading to an increase, with respect to the "no fluxes" solutions, of the growth rate and phase speed of unstable baroclinic waves. In particular, it was found that "... the faster deepening of the model's perturbations is a manifestation of their ability to organize warm and moist boundary layer air in a convergent circulation which continuously feeds a strong mesoscale updraft".

In order to provide some preliminary answer to the questions posed above, we will then proceed along a similar line, that is we will first include a simplified scheme of soil-atmosphere interaction in the E87 model, and then discuss the results from a set of analytical solutions. We do believe that approaching the problem in this way, rather than running simulations with "primitive equations" cloud models, will clarify, at least qualitatively, some important features of the large-scale soil moisture-precipitation feedback.

2. A semigeostrophic scheme for coupling soil moisture and baroclinic waves

2.1. *General formulation of the baroclinic model with soil interaction*

We consider the inviscid, Boussinesq semigeostrophic model of baroclinic instability described in E87. If (x, y, z) is a Cartesian reference frame, such that x and y are the zonal and meridional directions and z is a suitable function of pressure (Hoskins and Bretherton, 1972), the development of y-independent perturbations is studied, as forced by a base state zonal flow which is itself independent of y. The base state zonal flow is characterized by a vertical shear U_z which is uniform in the semigeostrophic coordinates defined as $(X, Y, Z, T) = (x + V_g/f, y - U_g/f, z, t)$:

$$U_g = U_z(Z - H). \tag{1}$$

The Coriolis parameter f is taken as constant and H is half the thickness of the troposphere, while the geostrophic wind components U_g and V_g are related to the potential temperature Θ (or dry entropy $S = C_p \ln \Theta$) by the thermal wind relations:

$$f\frac{\partial V_g}{\partial Z} = g\frac{\partial \ln \Theta}{\partial X}, \tag{2}$$

$$fU_z = -g\frac{\partial \ln \Theta}{\partial Y}. \tag{3}$$

The geostrophic meridional velocity V_g and all the ageostrophic velocities V_a, U_a and W, are assumed to be null in the initial base state. From the mass conservation equation, and considering y-independent perturbations, an ageostrophic streamfunction Ψ is defined, such that:

$$W = \frac{\partial \Psi}{\partial x} = \frac{\Xi}{f}\frac{\partial \Psi}{\partial X}, \tag{4}$$

$$U_a = -\frac{\partial \Psi}{\partial z} = -\frac{\Xi}{f^2}\frac{\partial V_g}{\partial Z}\frac{\partial \Psi}{\partial X} - \frac{\partial \Psi}{\partial Z}, \tag{5}$$

where $\Xi = f/(1 + \partial V_g/f\partial X)$ is the semigeostrophic approximation of the vertical component of the absolute vorticity. The same semigeostrophic approximation leads to the following simplified form for the zonal and meridional momentum equations:

$$fV_a = U_z\frac{\Xi}{f}\frac{\partial \Psi}{\partial X}, \tag{6}$$

$$\left(\frac{\partial}{\partial T} + U_g\frac{\partial}{\partial X}\right)V_g = f\frac{\partial \Psi}{\partial Z}. \tag{7}$$

Finally, defining the dry and equivalent potential vorticity in terms of dry and moist entropy (Θ_e is the equivalent potential temperature):

$$(Q, Q_e) = \frac{g\Xi}{f}\frac{\partial \ln(\Theta, \Theta_e)}{\partial Z}, \tag{8}$$

the entropy conservation equations may be written in the form:

$$g\left(\frac{\partial}{\partial T} + U_g\frac{\partial}{\partial X}\right)\ln(\Theta, \Theta_e) + (Q^*, Q_e)\frac{\partial \Psi}{\partial X} = \left(1, \frac{\Gamma_d}{\Gamma_m}\right)fU_zV_g. \tag{9}$$

Γ_d and Γ_m are the dry and moist adiabatic lapse rates. The reference potential vorticity Q^* in the dry entropy conservation equation, according to the condensation heat release scheme proposed in E87, is defined separately in saturated and unsaturated regions:

$$Q^* = \begin{cases} Q, & \text{unsaturated,} \\ \dfrac{\Gamma_m}{\Gamma_d} Q_e, & \text{saturated updraft.} \end{cases} \tag{10}$$

Finally, from Ertel's theorem, it is:

$$\frac{d(Q, Q_e)}{dT} = g \frac{\Xi}{f} \frac{\partial}{\partial Z} \frac{d \ln(\Theta, \Theta_e)}{dT}. \tag{11}$$

Such a scheme is based on the hypothesis that the vapor condensation is the only active diabatic process ($d \ln Q_e/dT = 0$). This may be considered as a valid hypothesis in the free atmosphere, at least at the spatial and temporal scales which are characteristic of the baroclinic instability dynamics. Nevertheless, we may argue that the latent and sensible heat exchanges that take place at the earth surface, largely dependent on the soil thermodynamics, still play a relevant role in the development of a baroclinic wave. It is well-known that the strength and the growth rate of such baroclinic waves are strongly controlled by the magnitude of the dry and equivalent potential vorticity, that is by the dry and moist entropy vertical profiles. We also expect that such profiles may undergo to sensible modifications, during the life-time of the baroclinic growth, because of the "injection" of heat and moisture from (to) the lower boundary, as found in Fantini (1991).

In Fantini (1991) the problem was restricted to the case of a warm sea lower boundary, so that there was always a positive flux of sensible and latent heat into the atmosphere, which could be modeled as a total flux proportional to the difference (constant in time) of the equivalent potential temperatures at the sea surface and at some height in the boundary layer. Here we are considering a quite different boundary situation, that is the soil, where: (a) the partitioning of the flux into sensible and latent is largely dependent on the soil saturation; (b) the surface layer is more rapidly adjusting to the various forcing, and it cannot be considered to be at constant temperature and necessarily warmer than the air.

In order to model the boundary fluxes with a simple scheme, we consider a well mixed atmospheric boundary layer of thickness $z^* \ll H$, and define inside of this region vertical-averaged values Θ_b and Θ_{eb} of the potential and equivalent potential temperatures, together with a reference moist air density ρ_b. If Q_h and LE are the sensible and latent heat fluxes from the soil (where L is the latent heat of condensation and E is the actual evapotranspiration), then we assume the following simplified boundary layer energy balance:

$$\frac{d \ln(\Theta_b, \Theta_{eb})}{dT} = \frac{1}{(\Theta_b, \Theta_{eb})} \frac{Q_h + (0, LE)}{\rho_b C_p z^*}. \tag{12}$$

At the same level of approximation, the soil thermodynamics may be represented by a simple energy balance of a surface layer of constant thickness Z_s. Calling with R_n any estimate of the net radiative energy flux into the soil, we simply write:

$$\frac{dT_s}{dT} = \frac{R_n - (Q_h + LE)}{\rho_s C_s Z_s}, \tag{13}$$

where ρ_s and C_s are representative values of the soil density and specific heat. The fluxes on the right end sides of eqs. (12) and (13) will be later expressed as general functions of the soil and atmospheric boundary layer states.

2.2. *Discretized non-dimensional model*

Analytical studies of similar problems (E87, Castelli et al., 1993) where based on the hypothesis of constant dry potential vorticity in unsaturated regions and constant equivalent potential vorticity in saturated regions. This hypothesis was justified by the absence, in such studies, of energy injection at the bottom of the flow domain. Because of the now considered temporal evolution of the dry and equivalent potential vorticity (eqs. 11–12), the model outlined in the previous section is highly non-linear. Numerical integration of the model's equation presents various difficulties. Among these, the discontinuous form of the variable Q^* in the free-atmosphere thermodynamics equations and of the energy fluxes. In order to capture the essential features of the model's solutions in the simplest way, we will focus our study to a two dimensional domain: this will be crudely discretized and the problem reduced to a set of coupled ordinary differential equations, which can be more easily studied by analytical techniques.

Before proceeding in such a simplification, we introduce non-dimensional variables, hereafter denote by lower-case letters. Defining a reference value for the zonal velocity as $U = U_z H/2$ and the non-dimensional vertical stability parameter

$\alpha = HQ_0/g$, the new non-dimensional variables are defined throughout the relations:

$$\begin{pmatrix} Q,\, Q_e,\, Q^* \\ \Xi \\ \Psi \\ (\ln\Theta, \ln\Theta_e) - \ln\Theta_0 \\ T_s \\ U_g \\ V_g \\ X \\ Z-H \\ T \\ Q_h,\, Q_h + LE,\, R_n \end{pmatrix} = \begin{pmatrix} Q_0 \\ f \\ HU \\ \alpha \\ \Theta_0 \\ 2U \\ HQ_0^{1/2} \\ HQ_0^{1/2}/f \\ H \\ HQ_0^{1/2}/fU \\ \rho_b C_p z^* f U \Theta_0 / HQ_0^{1/2} \end{pmatrix} \cdot \begin{pmatrix} q,\, q_e,\, q^* \\ \xi \\ \psi \\ \theta,\, \theta_e \\ \tau_s \\ z \\ v \\ x \\ z \\ t \\ f_{Qh},\, f_{QE},\, r_n \end{pmatrix} \tag{14}$$

Then the various equations that rule the free-atmosphere dynamics become:

$$\frac{\partial v}{\partial z} = \frac{\partial \theta}{\partial x}, \tag{15}$$

$$\frac{\partial v}{\partial t} + 2z\,\frac{\partial v}{\partial x} = \frac{\partial \psi}{\partial z}, \tag{16}$$

$$\frac{\partial(\theta, \theta_e)}{\partial t} + 2z\,\frac{\partial(\theta, \theta_e)}{\partial x} + (q^*, q_e)\,\frac{\partial \psi}{\partial x} = 2(1, \Gamma_d/\Gamma_m)\, v, \tag{17}$$

$$\frac{\mathrm{d}(q, q_e)}{\mathrm{d}t} = \xi\,\frac{\partial}{\partial z}\,\frac{\mathrm{d}(\theta, \theta_e)}{\mathrm{d}t}, \tag{18}$$

where:

$$\xi = \frac{1}{1 + \partial v/\partial x} \tag{19}$$

$$q^* = \begin{cases} q = \xi\,\dfrac{\partial \theta}{\partial z}, & \\ \quad \text{unsaturated,} & \\ \dfrac{\Gamma_m}{\Gamma_d}\, q_e = \dfrac{\Gamma_m}{\Gamma_d}\,\xi\,\dfrac{\partial \theta_e}{\partial z}, & \\ \quad \text{saturated updraft.} & \end{cases} \tag{20}$$

Defining also the non-dimensional parameter $\beta = \alpha(\rho_b C_p z^*)/(\rho_s C_s Z_r)$, the energy balance equations for the soil and the atmospheric boundary layers are:

$$\frac{\mathrm{d}\theta_b}{\mathrm{d}t} = f_{Qh}\exp(-\alpha\theta_b), \tag{21}$$

$$\frac{\mathrm{d}\theta_{eb}}{\mathrm{d}t} = f_{QE}\exp(-\alpha\theta_{eb}), \tag{22}$$

$$\frac{\mathrm{d}\tau_s}{\mathrm{d}t} = \beta(r_n - f_{QE}). \tag{23}$$

Many of the essential features of the just formulated model can be captured with a crude discretization of a two-dimensional flow domain. In particular, we consider the evolution of a y-independent baroclinic wave, whose half-wave length L is considered as a parameter. We then define representative values of the various quantities at appropriate levels, averaged horizontally over a length L. We assume that a single period of the flow domain can be subdivided in a region 1 where the vertical velocity is downdraft, corresponding to the cold anomaly of the perturbation, and a region 2 of updraft in the warm anomaly, both of length L (Fig. 1). In doing this, we are neglecting the contraction of the updraft region, with respect to the downdraft, due to the difference between the values of the dry and the equivalent potential vorticities. However this effect is relevant, as shown in E87, when the equivalent potential vorticity in the updraft region is much smaller than the dry one in the downdraft: This difference will be, as shown later, strongly reduced by the soil interaction, which has a stabilizing

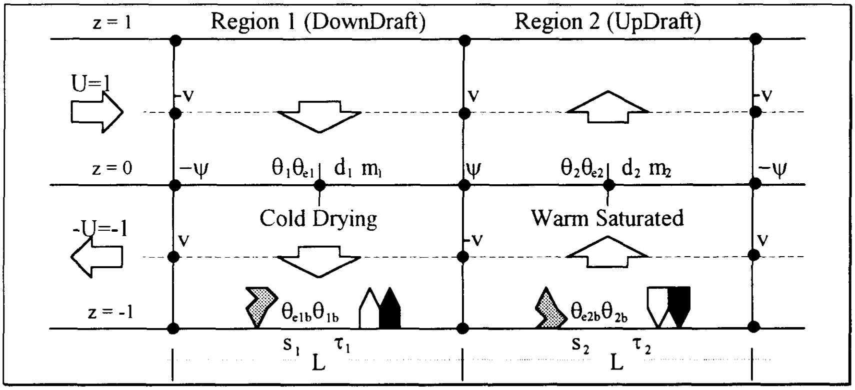

Fig. 1. Structure of the discretized model for the baroclinic wave of period $2L$. Variables, defined at the dotted nodes, are assumed to have symmetry properties.

effect on the moist vertical profile in the warm anomaly and de-stabilizing in the cold anomaly.

Fixed values $U = \pm 1$ of the zonal velocity are prescribed in the center of each layer ($z = \pm 1/2$), while 4 representative values of the perturbation meridional velocity v are defined at the same levels at the interfaces between region 1 and region 2. It is easy to show that such four velocities have the same absolute value, changing sign in a chessboard-like fashion. Two non-trivial values of the ageostrophic streamfunction are defined at the cross-points between the vertical layers and regions interfaces ($z = 0$), again found to have the same absolute value and opposite sign. We assume the convention that v and ψ are positive at the interface where the downdraft is on the left (with positive v in the upper layer). We also define average values of the free-atmosphere potential and equivalent potential temperatures (θ_1, θ_2) and $(\theta_{e1}, \theta_{e2})$ at the mid-level ($z = 0$) inside each region, where representative values of the dry potential vorticity, (d_1, d_2), and of the equivalent potential vorticity, (m_1, m_2), are also defined. Finally, the soil-atmosphere interface state (at $z = -1$), averaged inside each region, is represented by the values $(\theta_{b1}, \theta_{b2})$ and $(\theta_{eb1}, \theta_{eb2})$ of the boundary layer potential and equivalent potential temperatures, (τ_1, τ_2) of the soil absolute temperatures and (s_1, s_2) of the soil saturation.

We note that, in such a discretization, the boundary layer temperatures may be expressed as functions of the free-atmosphere temperatures and vertical lapse rates, these last being functions of the absolute and potential vorticity:

$$(\theta_{b1}, \theta_{eb1}) = (\theta_1, \theta_{e1}) - \frac{L + 2v}{L}(d_1, \gamma m_1), \tag{24}$$

$$(\theta_{b2}, \theta_{eb2}) = (\theta_2, \theta_{e2}) - \frac{L - 2v}{L}(d_2, \gamma m_2). \tag{25}$$

Using finite differencing for the spatial derivatives, upwind in the horizontal according to the sign of U, and upwind averaging for the forcing term in the thermodynamic equation, the following set of coupled ordinary differential equations is finally obtained (the superscript $\cdot$ stands for time derivative and $\gamma = \Gamma_d/\Gamma_m$):

$$\dot{v} = -\frac{2}{L}v - \psi, \tag{26}$$

$$\left(\dot{\theta}_1, \frac{1}{\gamma}\dot{\theta}_{e1}\right) = -2v - \frac{2}{L}(d_1, m_1)\,\psi, \tag{27}$$

$$\left(\dot{\theta}_2, \frac{1}{\gamma}\dot{\theta}_{e2}\right) = 2v + \frac{2}{L}(d_2, m_2)\,\psi, \tag{28}$$

$$(\dot{\tau}_1, \dot{\tau}_2) = \beta(r_{n1} - f_{QE1}, r_{n2} - f_{QE2}), \tag{29}$$

$$(\dot{d}_1, \gamma\dot{m}_1) = -(f_{Qh1}, f_{QE1}) \exp\left\{-\alpha\left[(\theta_1, \theta_{e1}) - \left(\frac{L + 2v}{L}\right)(d_1, \gamma m_1)\right]\right\}, \tag{30}$$

$$(\dot{d}_2, \gamma\dot{m}_2) = -(f_{Qh2}, f_{QE2}) \exp\left\{-\alpha\left[(\theta_2, \theta_{e2}) - \left(\frac{L-2v}{L}\right)(d_2, \gamma m_2)\right]\right\}, \tag{31}$$

where:

$$\psi = -\frac{4Lv}{L^2 + d_1 + m_2}. \tag{32}$$

3. Method of solution

Let us consider the following undisturbed base state:

$$\begin{pmatrix} v \\ \theta_1, \theta_2, d_1, d_2 \\ m_1, m_2 \\ \theta_{e1}, \theta_{e2} \\ \tau_1, \tau_2 \end{pmatrix} = \begin{pmatrix} 0 \\ D \\ M < D \\ \gamma M + \ln(S)/\alpha \\ 1 \end{pmatrix}, \tag{33}$$

where $S = \tau_{\text{sat}}(\tau = 1)$. The flux of sensible heat at the boundary between the soil and the atmosphere will be, in general, an approximate function of the difference between the absolute temperatures in the boundary layers:

$$f_{Qh} \approx f_{Qh}(\tau - \theta_b) = f_{Qh}(\tau, \theta, d, v). \tag{34}$$

In an analogous manner, the difference between the saturation temperatures will provide the estimate of the total (sensible plus latent) heat flux at its potential rate:

$$f_{QE\,\text{pot}} \approx f_{QE\,\text{pot}}(\tau_{\text{sat}} - \theta_{\text{eb}}) = f_{QE\,\text{pot}}(\tau, \theta_e, m, v). \tag{35}$$

The actual total flux will be controlled by the soil relative saturation s. In particular, it is a common assumption to relate the actual latent heat flux to its potential rate by the simple relation (Lowry, 1959):

$$LE = G(s, \text{sign}(LE_{\text{pot}}))\, LE_{\text{pot}}, \tag{36}$$

where $G \in [0, 1]$ is an increasing function of s if LE_{pot} is positive, and a decreasing function in the opposite case. We then obtain:

$$f_{QE} = (1 - G)\, f_{Qh} + G f_{QE\,\text{pot}}. \tag{37}$$

Assuming, as in E87, that the atmosphere is initially saturated, the undisturbed base state (33) implies that the sensible and total heat fluxes (34) and (37) are null for such a state. To consider it as an initial equilibrium solution, we have to introduce the further hypothesis that also the radiative flux is null for such a condition, while it will develop as the soil temperature changes.

On the basis of these assumptions, the growth of baroclinic disturbances may be studied by expanding the state variables as power series of the small amplitude δ of an initial perturbation in any of the variables:

$$\begin{pmatrix} v \\ \theta_1, \theta_2, d_1, d_2 \\ m_1, m_2 \\ \theta_{e1}, \theta_{e2} \\ \tau_1, \tau_2 \end{pmatrix} = \begin{pmatrix} 0 \\ D \\ M \\ \gamma M + \ln(S)/\alpha \\ 1 \end{pmatrix} + \sum_{n=1}^{\infty} \delta^n \begin{pmatrix} v_n \\ \theta_{n1}, \theta_{n2}, d_{n1}, d_{n2} \\ m_{n1}, m_{n2} \\ \theta_{ne1}, \theta_{ne2} \\ \tau_{n1}, \tau_{n2} \end{pmatrix}. \tag{38}$$

Expanding the various non-linear terms in the equations as Taylor series, the O(δ) approximation gives the following system of equations for the terms with $n = 1$:

$$\dot{v} \approx \frac{2(L^2 - D - M)}{L(L^2 + D + M)} v, \tag{39}$$

$$\dot{\theta}_1 \approx -\frac{2(L^2 - 3D + M)}{L^2 + D + M} v, \tag{40}$$

$$\dot{\theta}_2 \approx \frac{2(L^2 + D - 3M)}{L^2 + D + M} v, \tag{41}$$

$$\frac{1}{\gamma}\dot{\theta}_{e1} = -\frac{1}{\gamma}\dot{\theta}_{e2} \approx -\frac{2(L^2 + D - 3M)}{L^2 + D + M} v, \tag{42}$$

$$\frac{1}{\beta}\dot{\tau}_i \approx \frac{\partial r_{ni}}{\partial \tau_i}\tau_i - \left(\frac{\partial f_{QEi}}{\partial \tau_i}\tau_i + \frac{\partial f_{QEi}}{\partial \theta_i}\theta_i + \frac{\partial f_{QEi}}{\partial \theta_{ei}}\theta_{ei} + \frac{\partial f_{QEi}}{\partial d_i}d_i + \frac{\partial f_{QEi}}{\partial m_i}m_i + \frac{\partial f_{QEi}}{\partial v}v\right), \qquad i=1,2, \tag{43}$$

$$\dot{d}_i \approx -\left(\frac{\partial f_{Qhi}}{\partial \tau_i}\tau_i + \frac{\partial f_{Qhi}}{\partial \theta_i}\theta_i + \frac{\partial f_{Qhi}}{\partial d_i}d_i + \frac{\partial f_{Qhi}}{\partial v}v\right), \qquad i=1,2, \tag{44}$$

$$\gamma S\dot{m}_i \approx -\left(\frac{\partial f_{QEi}}{\partial \tau_i}\tau_i + \frac{\partial f_{QEi}}{\partial \theta_i}\theta_i + \frac{\partial f_{QEi}}{\partial \theta_{ei}}\theta_{ei} + \frac{\partial f_{QEi}}{\partial d_i}d_i + \frac{\partial f_{QEi}}{\partial m_i}m_i + \frac{\partial f_{QEi}}{\partial v}v\right), \qquad i=1,2. \tag{45}$$

We note that only the variable v appears in the first equation. It is then convenient to choose as initial conditions $v=1$ and $(\theta_1, \theta_2, ..., m_1, m_2)=0$. With these initial conditions, eqs. (39)–(42) have the simple solution:

$$v = \mathrm{e}^{\sigma t},$$

$$\begin{pmatrix}\theta_1\\ \theta_2\\ \theta_{e1}\\ \theta_{e2}\end{pmatrix} = \begin{pmatrix}-(1-\mu)\\ (1+\mu)\\ -\gamma(1+\mu)\\ \gamma(1+\mu)\end{pmatrix} \times L(\mathrm{e}^{\sigma t}-1), \tag{47}$$

where:

$$\sigma = \frac{2(L^2-D-M)}{L(L^2+D+M)}, \tag{48}$$

$$\mu = \frac{2(D-M)}{L^2-D-M}. \tag{49}$$

The other 6 equations form two independent systems of three equations each, whose solutions, derived in appendix A, may be expressed in the general form:

$$\begin{pmatrix}\tau_i\\ d_i\\ m_i\end{pmatrix} = \begin{pmatrix}A_{\tau i}\\ A_{di}\\ A_{mi}\end{pmatrix}(\mathrm{e}^{\sigma t}-1) + \begin{pmatrix}B_{\tau i}\\ B_{di}\\ B_{mi}\end{pmatrix}\mathrm{e}^{\sigma t} + \begin{pmatrix}C_{\tau i}\\ C_{di}\\ C_{mi}\end{pmatrix}\mathrm{e}^{\omega_{iC} t} + \begin{pmatrix}D_{\tau i}\\ D_{di}\\ D_{mi}\end{pmatrix}\mathrm{e}^{\omega_{iD} t} + \begin{pmatrix}E_{\tau i}\\ E_{di}\\ E_{mi}\end{pmatrix}\mathrm{e}^{\omega_{iE} t}, \qquad i=1,2.$$

The evolution of the baroclinic wave is mainly controlled by the evolution of the meridional velocity v. At the $O(\delta)$ level of approximation, which may be well representative of the initial growing stage, the evolution of v is dependent on the base state conditions only. At this stage we have a short-wave cutoff at $L=(D+M)^{1/2}$ and a maximum initial growing rate $\sigma_{\max} = 0.6006(D+M)^{-1/2}$ at $L=2.058(D+M)^{1/2}$. Later on, variations of d_1 and m_2 may become relevant, because of strong interaction with the soil, so that the growth rate and, as a consequence, the circulation at the time of the eventual frontal collapse will be affected as well.

To study the non-linear evolution beyond the initial stage, we analyze the $O(\delta^2)$ level of approximation, at which we have the following equation for v:

$$\dot{v} \approx \sigma v - \varepsilon \mathrm{e}^{\sigma t}(d_1 + m_2), \tag{51}$$

where

$$\varepsilon = \frac{4L}{(L^2+D+M)^2}, \tag{52}$$

Substituting $v = -\varepsilon \mathrm{e}^{\sigma t} u$, we obtain the simple equation for the new variable u:

$$\dot{u} = d_1 + m_2. \tag{53}$$

Setting a null initial condition for u, the following solution is obtained:

$$u = \frac{1}{\sigma}(A_{d1} + B_{d1} + A_{m2} + B_{m2})(e^{\sigma t} - 1)$$
$$+ \frac{C_{d1}}{\omega_{1C}}(e^{\omega_{1C}t} - 1) + \frac{C_{m2}}{\omega_{2C}}(e^{\omega_{2C}t} - 1)$$
$$+ \frac{D_{d1}}{\omega_{1D}}(e^{\omega_{1D}t} - 1) + \frac{D_{m2}}{\omega_{2D}}(e^{\omega_{2D}t} - 1)$$
$$+ \frac{E_{d1}}{\omega_{1E}}(e^{\omega_{1E}t} - 1) + \frac{E_{m2}}{\omega_{2E}}(e^{\omega_{2E}t} - 1)$$
$$- (A_{d1} + A_{m2})\, t. \tag{54}$$

As shown in appendix A, the sets of exponents $(\omega_{iC}, \omega_{iD}, \omega_{iE})$, $i = 1, 2$, come from the solution of a homogeneous systems of equations in the variables (τ_{si}, d_i, m_i). Such systems may be considered as representative of the evolution of the soil-atmosphere state in the absence of any dynamical and radiative forcing. We then expect that, with a reasonable formulation of the energy fluxes, no instability may develop in such an unforced condition. This is like to say that all the exponents $(\omega_{iC}, \omega_{iD}, \omega_{iE})$, $i = 1, 2$, are expected to have negative real parts. As t becomes large all the constant, linear and exponential terms with exponents $(\omega_{iC}, \omega_{iD}, \omega_{iE})$ in eq. (50) become negligible with respect to the term with exponent σ whenever this last one is positive (that is, whenever we expect to have a growing baroclinic wave). Then finally we may write, as t becomes large and the frontal collapse is approached, combining the $O(\delta)$ and the $O(\delta^2)$ solutions:

$$v \approx \delta e^{\sigma t}\left[1 - \frac{\varepsilon}{\sigma}(A_{d1} + B_{d1} + A_{m2} + B_{m2})\,\delta e^{\sigma t}\right]$$
$$= \delta e^{\sigma t}\left[1 - \frac{\varepsilon}{\sigma} A_v\, \delta e^{\sigma t}\right]. \tag{55}$$

Before proceeding to a more detailed analysis of the solutions, we observe that at the order $O(\delta)$ the evolution of the baroclinic dynamics is independent on the soil-atmosphere interaction. A the order $O(\delta^2)$ the dynamics becomes dependent on the soil-atmosphere interaction through the coefficients (A_{d1}, B_{d2}), which represent the $O(\delta)$ evolution of the dry potential vorticity in the region 1 of dry downdraft, and the coefficients (A_{m2}, B_{m2}), which represent the $O(\delta)$ evolution of the equivalent potential vorticity in the region 2 of saturated updraft. At the order $O(\delta)$ the evolution of the potential vorticity in the two regions is independent one on the other (their are coupled only through the $O(\delta)$ dynamics), while they become fully coupled at the order $O(\delta^2)$.

4. Specification of the boundary fluxes and analysis of solutions for extreme soil saturation

The solutions derived in the previous section have been expressed, so far, leaving the boundary energy and mass fluxes still to be specified. In order to proceed with a simple formulation of the model, it was assumed in eqs. (12) and (13) that the thickness of the soil and atmospheric boundary layers remain constant in time and space. Exchange of latent and sensible heat between the soil and the atmosphere are known to be dependent on the characteristic of the atmospheric boundary layer, and vice-versa. A variety of parameterizations have been proposed in the literature for the atmospheric boundary layer (i.e., Van Hulden and Holtslag, 1985), which all rely on the accurate estimation of the soil response to the solar radiation and hence on the account for the diurnal cycle. The model used here is far below such a level of detail, in particular with respect to the representation of the atmospheric and soil vertical profiles. We also stress again that what we are investigating are the possible feedbacks of soil moisture on precipitation through large-scale dynamics, such as cyclonic convergence, rather than through small scale deep convection. To this respect, we are interested in the boundary layer dynamics only as a "filter" between the soil and the troposphere, with no direct role in the precipitation occurrence. Finally, we note that in the numerical simulations of Fast and McCorcle (1991) the variability on the soil moisture distribution was found to have a significant effect on the average temperature and humidity of the boundary layer, but a much less relevant effect on its thickness. On the basis of these considerations, we assume the following simple forms for the sensible and potential total heat fluxes:

$$\frac{1}{\chi} f_{Qh} = \tau - \theta_b$$
$$= \tau - \exp\left\{\alpha\left[\theta - \left(\frac{L \pm 2v}{L}\right) d\right]\right\}, \tag{56}$$

$$\frac{1}{\chi} f_{QE\mathrm{pot}} = \tau_{\mathrm{sat}}(\tau) - \theta_{eb}$$

$$= \tau_{\mathrm{sat}}(\tau) - \exp\left\{\alpha\left[\theta_e - \gamma\left(\frac{L \pm 2v}{L}\right)m\right]\right\}. \quad (57)$$

The dimensionless parameter χ can be estimated as (Bras, 1990):

$$\chi = \frac{k^2 g}{z^* f Q_0^{1/2}}\left[\frac{U^*}{U \ln^2(z^*/z_0)}\right], \quad (58)$$

where k is the Von-Kàrmàn constant, U^* is a reference wind velocity inside the boundary layer and z_0 is the soil roughness. Given the atmospheric parameters specified in Table 1 and common values for the soil surface properties (i.e., Peixoto and Oort, 1992), we may assume $\chi = 10^1 - 10^2$ and $\beta \approx 10^{-1}$.

The specification of the net radiative flux into the soil is somewhat more problematic, having taken the crude assumption of null radiative forcing for the base state. Again, given the simplified framework of the model, we will retain its dependence on the soil temperature only, neglecting all the other factors, such as the changing atmospheric conditions and the soil-moisture dependent albedo. Given then the initial equilibrium condition and referring to the Stefan-Boltzman law, we write:

$$r_n = \frac{\lambda}{4}(1 - \tau_s^4), \quad (59)$$

where the dimensionless parameter λ may be estimated in the range $10^{-2} - 1$.

Having specified the various fluxes in such a way, their partial derivatives with respect to the various state variables are, at order $O(\delta)$ of approximation:

$$\frac{\partial f_{Qh1}}{\partial \tau_1} = \frac{\partial f_{Qh2}}{\partial \tau_2} = \gamma \frac{\partial f_{QE\mathrm{pot1}}}{\partial \tau_1} = \gamma \frac{\partial f_{QE\mathrm{pot2}}}{\partial \tau_2} = \chi, \quad (60)$$

$$\frac{\partial f_{Qh1}}{\partial \theta_1} = \frac{\partial f_{Qh2}}{\partial \theta_2} = \frac{1}{S}\frac{\partial f_{QE\mathrm{pot1}}}{\partial \theta_{e1}}$$

$$= \frac{1}{S}\frac{\partial f_{QE\mathrm{pot2}}}{\partial \theta_{e2}} = -\alpha\chi, \quad (61)$$

$$\frac{\partial f_{Qh1}}{\partial d_1} = \frac{\partial f_{Qh2}}{\partial d_2} = \frac{1}{\gamma S}\frac{\partial f_{QE\mathrm{pot1}}}{\partial m_1}$$

$$= \frac{1}{\gamma S}\frac{\partial f_{QE\mathrm{pot2}}}{\partial m_2} = \alpha\chi, \quad (62)$$

$$\frac{1}{D}\frac{\partial f_{Qh1}}{\partial v} = -\frac{1}{D}\frac{\partial f_{Qh2}}{\partial v} = \frac{1}{\gamma SM}\frac{\partial f_{QE\mathrm{pot1}}}{\partial v}$$

$$= -\frac{1}{\gamma SM}\frac{\partial f_{QE\mathrm{pot2}}}{\partial v} = \frac{2\alpha\chi}{L}, \quad (63)$$

$$\frac{\partial r_{n1}}{\partial \tau_1} = \frac{\partial r_{n2}}{\partial \tau_2} = -\lambda. \quad (64)$$

As stated in eq. (37), the actual total heat flux may be expressed as a weighted average, through the function G of the soil saturation, of the sensible and potential total heat fluxes. For the seek of conciseness, we will analyze in more detail the solutions corresponding to the four possible extreme soil moisture distributions. Keeping in mind that we expect such fluxes to be positive in region 1, where the atmosphere is cooling and drying as the baroclinic wave grows, and the opposite in region 2, such four configurations may be specified as follows.

DW: totally dry soil in region 1 and a totally wet soil in region 2. No possibility of either evaporation or condensation from/into the soil ($G(s_1) = G(s_2) = 0$).

WD: Totally wet soil in region 1 and totally dry soil in region 2. Evaporation and condensation from/into the soil at their potential rate ($G(s_1) = G(s_2) = 1$).

WW: Totally wet soil in both regions 1 and 2. Evaporation from the soil at its potential rate ($G(s_1) = 1$) and no condensation into the soil ($G(s_2) = 0$).

Table 1. *Values of the atmospheric parameters assumed for the undisturbed base state*

Θ_0	280°K
Q_0	$1.36 \times 10^{-4}\ \mathrm{s}^{-2}$
f	$10^{-4}\ \mathrm{s}^{-1}$
U	$15\ \mathrm{m\ s}^{-1}$
H	$5 \times 10^3\ \mathrm{m}$
k	0.4
g	$9.81\ \mathrm{m\ s}^{-2}$

DD: Totally dry soil in both regions 1 and 2. Condensation into the soil at its potential rate ($G(s_2)=1$) and no evaporation from the soil ($G(s_1)=0$).

Main goal of this analysis is to establish which one, among the four extreme soil moisture distributions, is more "favorable" in terms of perturbation growth and rainfall production.

The coefficients of the $O(\delta)$ solutions for these extreme cases are reported in Appendix B. Focusing the attention on the solution for v as expressed in eq. (55), we are mainly interested in the sum of coefficients $A_v = A_{d1} + B_{d1} + A_{m2} + B_{m2}$. From the results in Appendix B the following specific results are obtained:

$$\begin{cases} G(s_1)=0, \\ A_{d1}+B_{d1} = -\dfrac{\left(\lambda+\dfrac{\sigma}{\beta}\right)\left[\alpha(1-\mu)L+\dfrac{2\alpha D}{L}\right]}{\left(\lambda+\dfrac{\sigma}{\beta}\right)\left(\dfrac{\sigma}{\chi}+\alpha\right)+\sigma}, \\ G(s_1)=1, \\ A_{d1}+B_{d1} = \\ = -\dfrac{\left[\left(\lambda+\dfrac{\sigma}{\beta}\right)\left(\dfrac{\sigma}{\chi}+\alpha\right)+\dfrac{\sigma}{\gamma}\right]\left[\left(\dfrac{\sigma}{\chi}+\alpha\right)(1-\mu)L+\dfrac{2\alpha D}{L}\right] - \gamma S\sigma\left[\alpha(1+\mu)L+\dfrac{2\alpha M}{L}\right]}{\left(\dfrac{\sigma}{\chi}+\alpha\right)\left[\left(\lambda+\dfrac{\sigma}{\beta}\right)\left(\dfrac{\sigma}{\chi}+\alpha\right)+\dfrac{\sigma}{\gamma}\right]}, \\ G(s_2)=0, \\ A_{m2}+B_{m2} = \dfrac{\gamma S\left(\lambda+\dfrac{\sigma}{\beta}\right)\left[\alpha(1+\mu)L+\dfrac{2\alpha D}{L}\right]}{\left(\lambda+\dfrac{\sigma}{\beta}\right)\left(\dfrac{\sigma}{\chi}+\alpha\right)+\sigma}, \\ G(s_2)=1, \\ A_{m2}+B_{m2} = \dfrac{\gamma\left(\lambda+\dfrac{\sigma}{\beta}\right)\left[\alpha(1+\mu)L+\dfrac{2\alpha M}{L}\right]}{\gamma\left(\lambda+\dfrac{\sigma}{\beta}\right)\left(\dfrac{\sigma}{\chi}+\alpha\right)+\sigma}. \end{cases} \quad (65)$$

The main source of uncertainty, in the model under investigation, is the formulation of the net radiative flux at the soil surface, here represented by the parameter λ. We will then analyze, from now on, the just formulated solutions as functions of both the parameter λ and the baroclinic wavelength L. The other parameters are taken as $(D, M, \alpha, \beta, \chi) = (1, 0.5, 0.0693, 0.1, 20)$. A linear short-wave cutoff is expected at $L = 1.225$.

Fig. 2 shows the contour plots of the four parameters sums of eq. (65), corresponding to the two extreme soil moisture distributions in each one of the two regions of the model's periodic domain (Fig. 1). We know, from eq. (55), that the larger positive is the sum $A_v = A_{d1} + B_{d1} + A_{m2} + B_{m2}$, the slower is the growth of the baroclinic wave beyond the initial linear stage. The opposite when A_v becomes negative. As shown in the plots (a) and (b) of Fig. 2, the sum $A_{d1} + B_{d1}$ is negative: the air is cooling down in region 1 as the perturbation grows, so that a positive heat flux from the soil is expected, which will tend to reduce the atmospheric dry vertical stability. In both cases the sum becomes more negative for increasing L and decreasing λ. In the absence of evapotranspiration (dry soil) the adjusting mechanism is much less efficient, resulting in an increase of heat flux and hence a decrease, with respect to the case with wet soil, of the sum $A_{d1} + B_{d1}$. The opposite occurs for the sum $A_{m2} + B_{m2}$ in region 2 (plots (c) and (d)), which are always found to be positive. The atmosphere is there warming up, while the dynamics is sensitive to the moist vertical stability. The total heat flux, now directed into the soil, is again dependent on the soil moisture content. In the case of wet soil, downward transport of moisture from the atmosphere into the soil is prevented, resulting in a less stabilizing effect and hence in smaller values of $A_{m2} + B_{m2}$.

We then have a first conclusion that soil dryness in region 1 is in favor of the baroclinic wave growth and the same for soil wetness in region 2, where precipitation is going to occur. How these tendencies combine together in the four extreme configurations DW, WD, WW and DD is shown in Fig. 3, where the contour plots of the coefficient A_v are reported. First, we observe that when the soil in region 1 is wet (WW and WD), because of the more efficient soil response, A_v is much more sensitive to the solar radiation than in the DD and DW cases. In general, such a dependence tends to

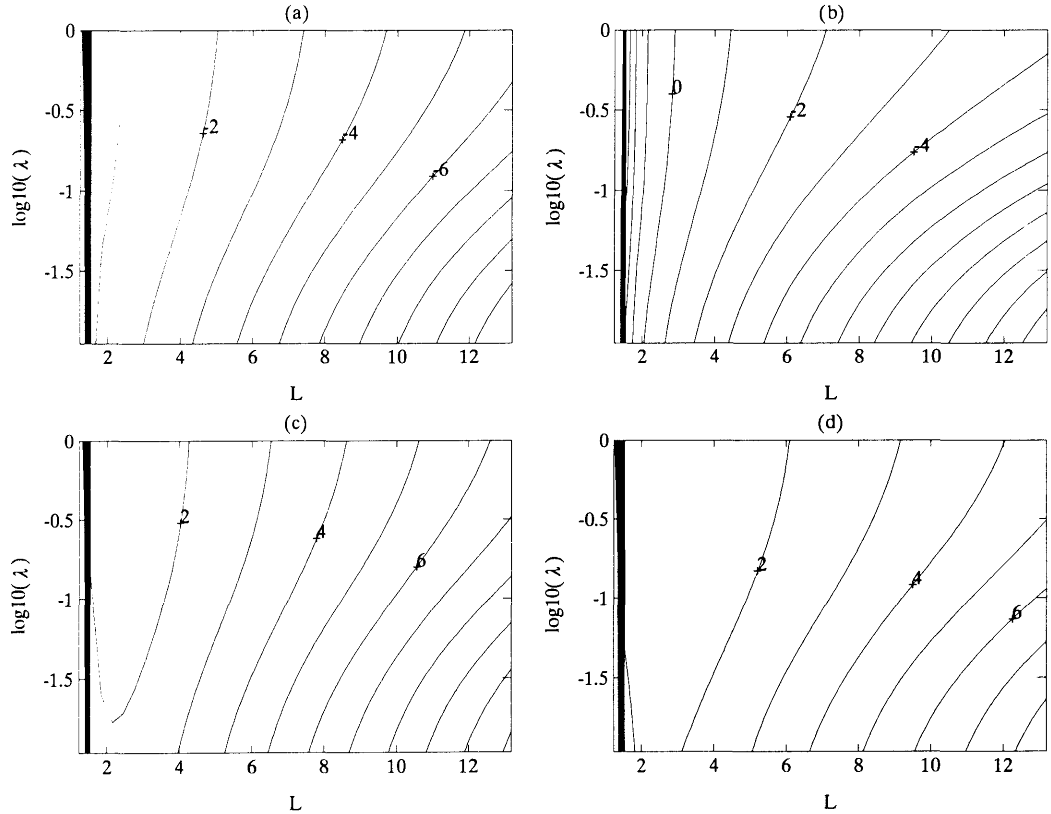

Fig. 2. Contour plots, for varying half-wavelength L and radiative flux parameter λ, of the following sums of coefficients: (a) $A_{d1}+B_{d1}$ for $G(s_1)=0$. (b) $A_{d1}+B_{d1}$ for $G(s_1)=1$. (c) $A_{m2}+B_{m2}$ for $G(s_2)=1$. (c) $A_{m2}+B_{m2}$ for $G(s_2)=0$.

disappear as L decreases toward the short-wave cutoff. In the DW case the coefficient A_v is almost always smaller than in all the other cases, with negative values, that is an accelerated growth, when L exceeds 4.3. In the DD case A_v is always positive. WW has the largest A_v values for short L, but smaller values than DD and WD as L increases and λ decreases: for a limited region of L around 0.8 and λ toward 0.01, A_v is smaller in WW than in all the other cases.

A more meaningful measure of the dynamics of the baroclinic wave, and also more interesting from the point of view of the rainfall production, is given by the timing of the frontal collapse. A frontal discontinuity is obtained, in the framework of the semigeostrophic theory, whenever a singularity occurs in the absolute vorticity field (Hoskins and Bretherton, 1972). In the discretized model discussed here this condition is matched when the meridional velocity reaches the value $v=L/2$. The time needed to reach the frontal collapse will depend, in absolute terms, by the amplitude δ of the perturbation at $t=0$. We may then consider, as a δ-independent measure of the frontal collapse timing, the factor $\delta\exp(\sigma t_c)$, where t_c is the time at which $v=L/2$ is reached. Eq. (55) gives a second order equation for such a factor, from where we obtain:

$$\delta e^{\sigma t_c}=\frac{1-\sqrt{1-2L\varepsilon A_v}}{2\varepsilon A_v}. \tag{66}$$

This result shows that, even for positive values of σ, the reaching of the frontal collapse may be prevented if $A_v>1/(2\varepsilon L)$: an initially growing

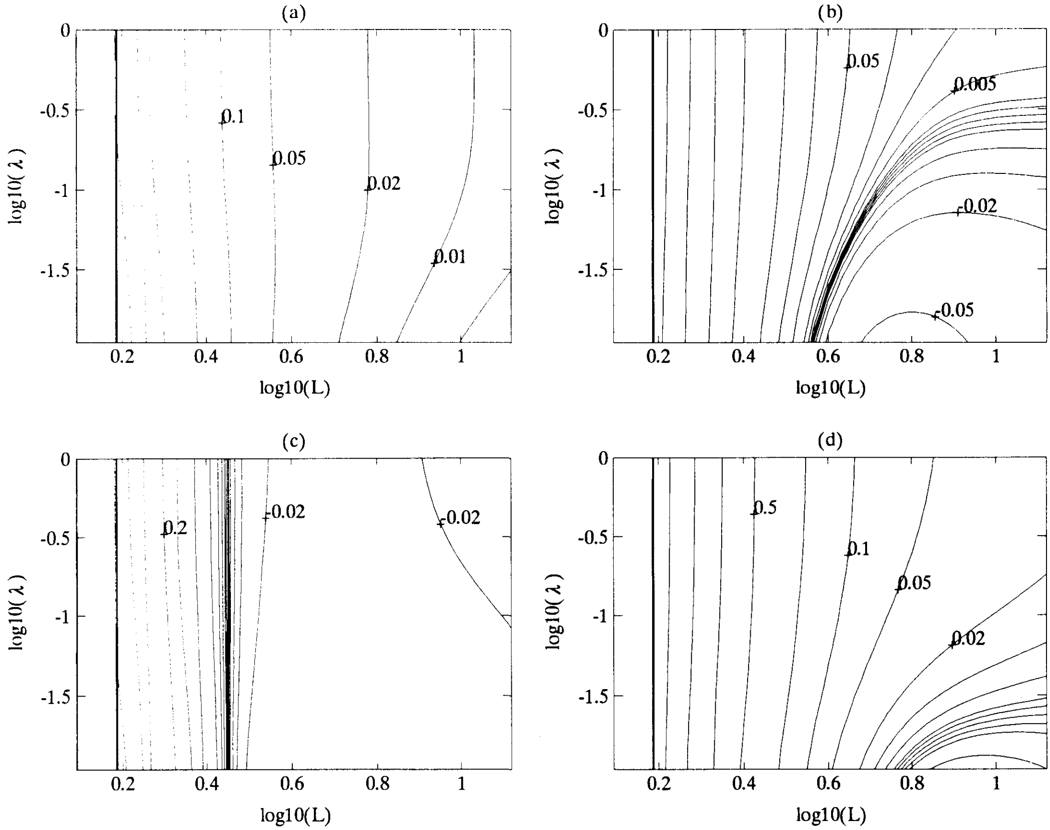

Fig. 3. Contour plots, for varying half-wavelength L and radiative flux parameter λ, of the coefficient A_v of eq. (55) and the following soil moisture configurations: (a) DD, (b) WW, (c) DW, (d) WD.

wave is dumped down, in such cases, before the reaching of the frontal collapse by the stabilizing soil-atmosphere interaction, defining this way a "non-linear cutoff". Contour plots of the factor $\delta \exp(\sigma t_c)$ are shown in Fig. 4. Dotted areas represent values of the parameters L and λ for which the frontal collapse is never reached. By observing the extension of these areas and the values of the contour lines it is clear how the DW and WD configurations are, respectively, the more favorable and the less favorable in terms of frontal collapse occurrence. The comparison between the intermediate cases DD and WW is dependent on the wavelength L: low values of L favor the DD configuration, the opposite for high values of L.

In the linear theory with no soil-atmosphere interaction, the growth speed of the baroclinic wave is simply represented by the instability exponent σ. For the non-linear solution (55) an equivalent measure of the growth speed may be given by the inverse of the last doubling time t_d before the frontal collapse, that is the inverse of the time needed to go from $v = L/4$ to $v = L/2$. With no soil interaction it would be simply $1/t_d = \sigma/\log(2)$. From eq. (55) we now obtain:

$$\frac{1}{t_d} = \frac{\sigma}{\ln(1-\sqrt{1-2L\varepsilon A_v}) - \ln(1-\sqrt{1-L\varepsilon A_v})}. \tag{67}$$

When expressed as a function of L, $1/t_d$ may be considered as equivalent to the spectra of the non-linear baroclinic instability in the presence of soil-atmosphere interaction. This may be then compared to the spectra $\sigma(L)$ obtained by the linear

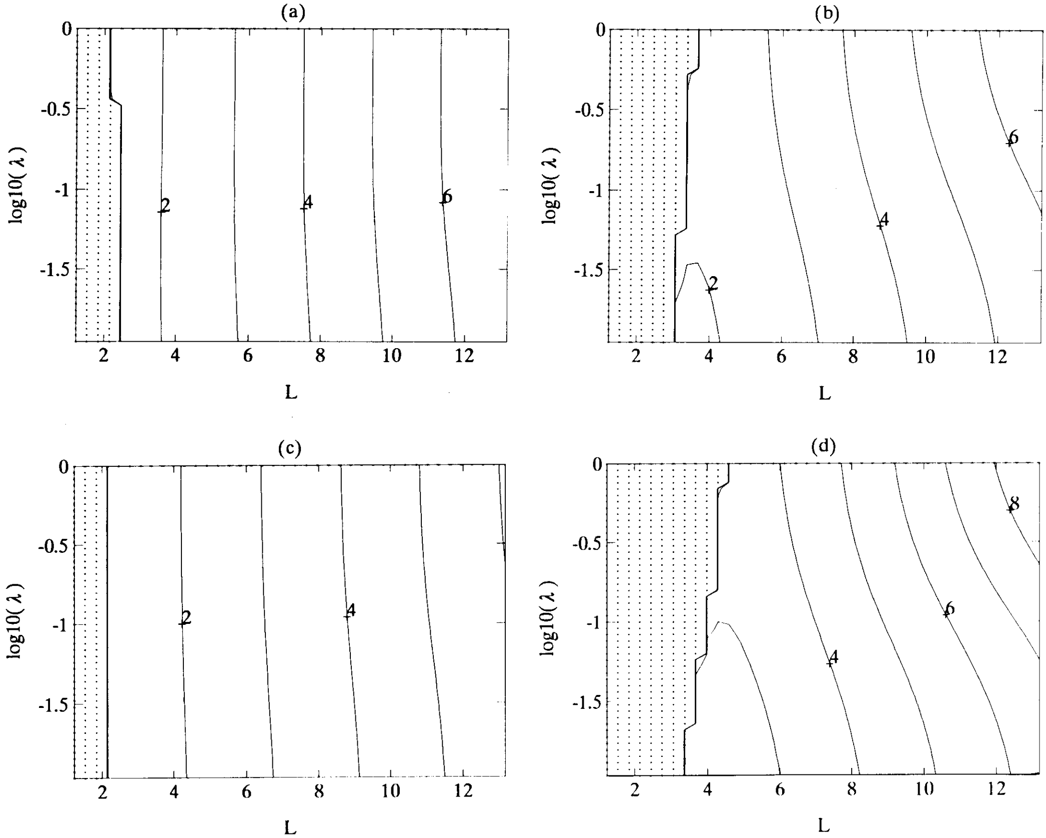

Fig. 4. As in Fig. 3, but for the factor $\delta \exp(\sigma t_c)$.

theory. Such a comparison is presented in Fig. 5a for a low value of the parameter λ. The DW case shows the smaller difference with respect to the linear case. The more evident difference is that the short-wave cutoff is moved toward higher values of L and it becomes discontinuous: the frontal collapse is either approached with a finite speed or never reached. Also the peak of the spectra is moved toward higher values of L, and the evolution is slowed/accelerated, with respect to the linear case, when L is below/above the peak value. The DD case is characterized by similar values of L in terms of peak and cutoff, but with values of $1/T_d$ which are smaller than in both the DW and the linear cases. Finally, in both WW and the WD cases the peak and cutoff L values are more than doubled, while the WD one shows values of $1/T_d$ which are the lowest for all the L range. The same specters, but for a much higher value of λ, are presented in Fig. 5b. Main difference with Fig. 5a is that now the DD and WW cases are inverted, in terms of the magnitude of $1/T_d$, when L exceeds a certain value. Both the DW and WW cases are now accelerated, with respect to the linear case, when L exceeds the corresponding peak value.

As stated in the introduction, the main goal of the present study is to analyze the possible feedback of soil moisture on its own forcing, that is on the precipitation. To this purpose, we may define a conceptual precipitation index R, as representative of the rainfall potential associated to the growth of a baroclinic wave up to the formation of an atmospheric front. We expect, on a qualitative basis, that such a rainfall potential is proportional to the magnitude of the updraft velocity in the saturated region and inversely related to the moist

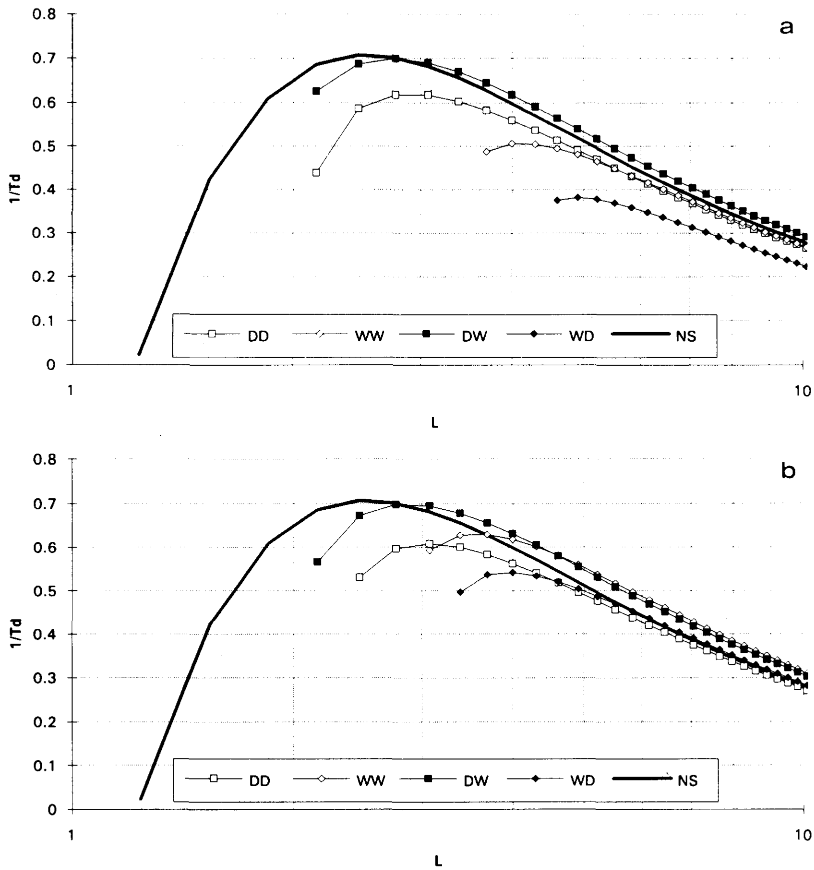

Fig. 5. Inverse of the last doubling time t_d before the reaching of the frontal collapse, for $\lambda = 10^{-2}$ (a) and $\lambda = 1$ (b), as a function of the half-wavelength L. The solid curve (NS) is relative to the linear solution with no soil-atmosphere interaction.

stability in the same region. In region 2 of saturated updraft the surface fluxes are such that the stability is progressively increased, we may then simply define $R = w_2/m_2$, where, being $w_2 = 2\psi/L$ at the mid troposphere:

$$w_2 = \frac{4L}{L^2 + D + M + \sigma/2\varepsilon(1 - \sqrt{1 - 2L\varepsilon A_v})}, \quad (68)$$

$$m_2 = M + (A_{m2} + B_{m2}) \left[\frac{1 - \sqrt{1 - 2L\varepsilon A_v}}{2\varepsilon A_v} \right]. \quad (69)$$

The values of R obtained for $\lambda = 0.01$ at the time of the frontal collapse are plotted in Fig. 6a. All the four cases with soil-atmosphere interaction show values of R which are strongly reduced with respect to the linear solution. This because of the above mentioned stabilizing effect of the surface fluxes in region 2, as shown by eq. (69) and Figs. 2 and 3. Again, the DW configuration is characterized by the higher values of R, and the WD by the lower ones. Despite the fact that, for low values of λ, the DD evolution is faster than the WW one, R is higher in the WW case for the values of L where both configurations allows for the reaching of the frontal collapse. In particular, as L increases no much difference exist among the precipitation index of the DW and WW configurations (or the DD and WD), highlighting the prevalent role of the moisture state in region 2 from the point of view of the rainfall production. Such differences are even more reduced for $\lambda = 1$ (Fig. 6b), with a general decrease of R because of the increased strength of the surface fluxes.

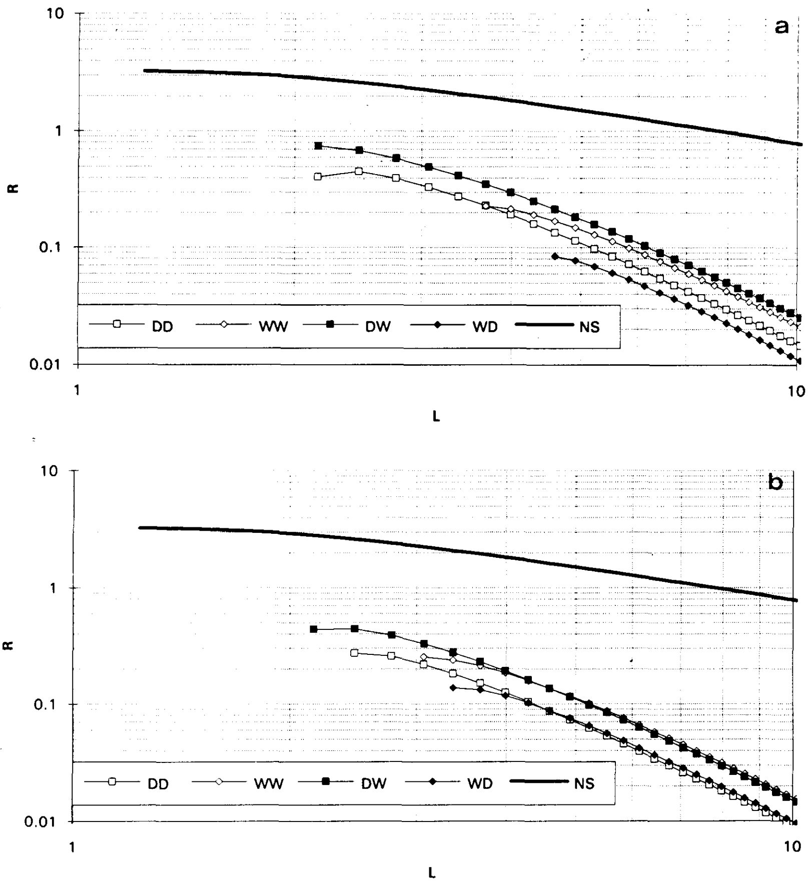

Fig. 6. Rainfall potential R at the time of the frontal collapse, for $\lambda = 10^{-2}$ (a) and $\lambda = 1$ (b), as a function of the half-wavelength L. The solid curve (NS) is relative to the linear solution with no soil-atmosphere interaction.

5. Conclusions

It has been recognized by many authors that the dynamical coupling of rainfall and soil moisture distributions plays an important role in the existence of large-scale spatial patterns of hydrological and climatological variables. This is a crucial issue in the understanding of the heterogeneity of the continental climates. As a step toward the study of such dynamical coupling, the attention has been focused on a more physically based representation of a specific mechanism of large-scale interaction between soil moisture and atmospheric processes. A wide literature addressing the relevant role of the atmospheric processes such as the moisture recycling and large scale transport, the interaction between an atmospheric moist baroclinic wave and the underlying soil has been chosen as a first reference dynamical scheme.

Starting from the inviscid semigeostrophic equations for the evolution of a meridionally independent baroclinic disturbance in the moist atmosphere, an ideal fluid-dynamical model has been adopted. A simplified, but quite general, scheme for the representation of the mass and energy exchanges between the soil and the atmospheric boundary layer has been included, in order to model the land-atmosphere coupling. Relying on a crude, but still consistent, discretization of the domain, the model is re-formulated in terms of coupled non-linear ordinary differential equations. Starting from a uniform zonal shear condition in the free atmosphere, and assuming an initial thermal equilibrium between the soil and the atmospheric boundary layer, the non-linear growth of baroclinic disturbances is modeled, up to the time of the frontal collapse, as a non-linear instability problem. Analytical solutions are then derived, as functions of the partial derivatives of the surface soil-controlled fluxes with respect to the various state variables. Such solutions, in the form reported form eq. (50) to eq. (55), may be considered as general to some extent: a variety of surface flux parameterizations may be used to estimate the terms which are lived unexplicited in the various linear systems of Appendix A.

A particular flux parameterization, widely adopted in many hydrometeorological and climatological studies, has been then chosen to analyze in some detail the solutions, restricting such an analysis to the four possible extreme soil moisture distributions. Given the difficulty in estimating the radiative surface flux as a function of the atmospheric base state, its representative magnitude has been chosen, together with the baroclinic perturbation wavelength $2L$, as a free parameter to test the solutions behavior.

Using such an approach, the question has been addressed about to which extent and through which mechanisms a heterogeneous soil moisture distribution affects the evolution of the baroclinic waves, and in particular the estimate of the potential precipitation. The main results may be summarized as follows.

The interaction between the land and the atmosphere has both a local effect and a large scale effect. The local effect consists in modifying the vertical lapse rates of dry and equivalent potential temperatures, as given by the solutions at the first level of approximation in the perturbation initial amplitude. At the second-order of approximation, which becomes relevant as the frontal collapse is approached, the perturbation growth is strongly affected by the modified vertical lapse rates, so that the land-atmosphere interaction may be said to influence the whole large scale dynamics.

In particular, the growth of the baroclinic wave is expected to be as much faster as smaller is the sum of the dry potential vorticity in region 1 (cold drying downdraft) and the equivalent potential vorticity in region 2 (warm saturated updraft). How much these quantities are modified is strictly dependent on the magnitude of the various surface fluxes, which are partitioned among sensible and latent according to the soil moisture content. When the soil in region 1 is dry, all the energy exchange with the atmosphere needed to cool down the soil is in the form of sensible heat, resulting in a much lower value of the dry potential vorticity in the same region. The land-atmosphere interaction in region 1 tends to accelerate the dynamics, and the more the soil is dry, the larger is the acceleration. In region 2, where the fluxes are directed into the soil and the moist potential vorticity is the concern, the land-atmosphere interaction tends to slow down the dynamics through both the latent and sensible heat fluxes. When the soil in region 2 is wet, the downward moisture transport is prevented, resulting in a smaller total flux and hence a weaker slow down of the perturbation growth. It is then clear how the DW soil moisture configuration is the one more in favor of the baroclinic dynamics, while the WD has the opposite effect. The relative relevance of the land-atmosphere interaction in the two regions is quite sensitive to both the magnitude of the radiative parameter λ and the wavelength $2L$. The interaction in region 1 prevails for most of the cases, favoring the DD configuration with respect to the WW. The opposite occurs when L is large and λ is very small. From the point of view of the rainfall potential, defined as proportional to the vertical velocity and to the inverse of the moist potential vorticity in region 2, the land-atmosphere interaction is more relevant in region 2 than in region 1, where also the precipitation itself is going to occur: the DW and WW cases lead to a higher rainfall estimate than the WD and DD.

These results provide a clear hint for the existence of a positive feedback of soil moisture on precipitation. Such a feedback is both local, because of the increased rainfall potential when the precipitation is going to occur on a wet soil, and spatially structured, because of the more accelerated dynamics when the soil under the warm precipitating anomaly is wet and the soil under the cold dry anomaly is dry.

6. Acknowledgments

The present study was partially supported by US-NFS (EAR-9120368) and NASA (NAGW-4171).

APPENDIX

(A) Coefficients of the general solution $O(\delta)$

We consider the system of three ordinary differential equations, derived from eqs. (43)–(47), where the subscript i has been dropped and the coefficients on the right-hand side of eq. (47) have been replaced by μ_d (in the place of $\mp(1\mp\mu)L$) and by μ_e (in the place of $\mp(1+\mu)L$):

$$\frac{1}{\beta}\dot{\tau}+\left(\frac{\partial f_{QE}}{\partial\tau}-\frac{\partial r_n}{\partial\tau}\right)\tau+\frac{\partial f_{QE}}{\partial d}d+\frac{\partial f_{QE}}{\partial m}m = \left[\mu_d\frac{\partial f_{QE}}{\partial\theta}+\gamma\mu_e\frac{\partial f_{QE}}{\partial\theta_e}\right](e^{\sigma t}-1)-\frac{\partial f_{QE}}{\partial v}e^{\sigma t}, \tag{A.1}$$

$$\dot{d}+\frac{\partial f_{Qh}}{\partial d}d+\frac{\partial f_{Qh}}{\partial\tau}\tau =\mu_d\frac{\partial f_{Qh}}{\partial\theta}(e^{\sigma t}-1)-\frac{\partial f_{Qh}}{\partial v}e^{\sigma t}, \tag{A.2}$$

$$\gamma S\dot{m}+\frac{\partial f_{QE}}{\partial m}m+\frac{\partial f_{QE}}{\partial\tau}\tau+\frac{\partial f_{QE}}{\partial d}d = \left[\mu_d\frac{\partial f_{QE}}{\partial\theta}+\gamma\mu_e\frac{\partial f_{QE}}{\partial\theta_e}\right](e^{\sigma t}-1)-\frac{\partial f_{QE}}{\partial v}e^{\sigma t}, \tag{A.3}$$

with all null initial conditions.

The system (A.1)–(A.3) has the particular solution:

$$\begin{pmatrix}\tau\\ d\\ m\end{pmatrix}=\begin{pmatrix}A_\tau\\ A_d\\ A_m\end{pmatrix}(e^{\sigma t}-1)+\begin{pmatrix}B_\tau\\ B_d\\ B_m\end{pmatrix}e^{\sigma t}, \tag{A.4}$$

where the coefficients are found solving the following sequence of two linear systems:

$$\begin{pmatrix}\frac{\partial f_{QE}}{\partial\tau}-\frac{\partial r_n}{\partial\tau} & \frac{\partial f_{QE}}{\partial d} & \frac{\partial f_{QE}}{\partial m}\\ \frac{\partial f_{Qh}}{\partial\tau} & \frac{\partial f_{Qh}}{\partial d} & 0\\ \frac{\partial f_{QE}}{\partial\tau} & \frac{\partial f_{QE}}{\partial d} & \frac{\partial f_{QE}}{\partial m}\end{pmatrix}\begin{pmatrix}A_\tau\\ A_d\\ A_m\end{pmatrix} = \begin{pmatrix}\mu_d\frac{\partial f_{QE}}{\partial\theta}+\mu_e\frac{\partial f_{QE}}{\partial\theta_e}\\ \mu_d\frac{\partial f_{Qh}}{\partial\theta}\\ \mu_d\frac{\partial f_{QE}}{\partial\theta}+\mu_e\frac{\partial f_{QE}}{\partial\theta_e}\end{pmatrix}, \tag{A.5}$$

$$\begin{pmatrix}\frac{\partial f_{QE}}{\partial\tau}-\frac{\partial r_n}{\partial\tau}+\frac{\sigma}{\beta} & \frac{\partial f_{QE}}{\partial d} & \frac{\partial f_{QE}}{\partial m}\\ \frac{\partial f_{Qh}}{\partial\tau} & \frac{\partial f_{Qh}}{\partial d}+\sigma & 0\\ \frac{\partial f_{QE}}{\partial\tau} & \frac{\partial f_{QE}}{\partial d} & \frac{\partial f_{QE}}{\partial m}+\gamma S\sigma\end{pmatrix} \times\begin{pmatrix}B_\tau\\ B_d\\ B_m\end{pmatrix}=-\begin{pmatrix}\frac{\partial f_{QE}}{\partial v}+\frac{\sigma}{\beta}A_\tau\\ \frac{\partial f_{Qh}}{\partial v}+\sigma A_d\\ \frac{\partial f_{QE}}{\partial v}+\gamma S\sigma A_m\end{pmatrix}. \tag{A.6}$$

To match the null initial condition, we have to add to the particular solution (A.4) the solution of the homogeneous system associated to (A.1)–(A.3). Such a solution may be written in the general form:

$$\begin{pmatrix}\tau\\ d\\ m\end{pmatrix}=\begin{pmatrix}C_\tau\\ C_d\\ C_m\end{pmatrix}e^{\omega_C t}+\begin{pmatrix}D_\tau\\ D_d\\ D_m\end{pmatrix}e^{\omega_D t}+\begin{pmatrix}E_\tau\\ E_d\\ E_m\end{pmatrix}e^{\omega_E t}, \tag{A.7}$$

where the exponents $(\omega_C, {}_D, \omega_E)$ are the roots of the cubic equation obtained by setting to zero the following determinant:

$$\begin{vmatrix}\omega+\frac{\partial f_{QE}}{\partial\tau}-\frac{\partial r_n}{\partial\tau} & \frac{\partial f_{QE}}{\partial d} & \frac{\partial f_{QE}}{\partial m}\\ \frac{\partial f_{Qh}}{\partial\tau} & \frac{\omega}{\beta}+\frac{\partial f_{Qh}}{\partial d} & 0\\ \frac{\partial f_{QE}}{\partial\tau} & \frac{\partial f_{QE}}{\partial d} & \gamma S\omega+\frac{\partial f_{QE}}{\partial m}\end{vmatrix}=0. \tag{A.8}$$

Finally, the various coefficients in (A.7) are found equating similar terms in two of the eqs. (A.1)–(A.3) and imposing the null initial condition:

$$\begin{pmatrix}
\frac{\partial f_{Qh}}{\partial \tau} & \omega_C+\frac{\partial f_{Qh}}{\partial d} & 0 & 0 & 0 & 0 & 0 & 0 & 0 \\
\frac{\partial f_{QE}}{\partial \tau} & \frac{\partial f_{QE}}{\partial d} & \gamma S\omega_C+\frac{\partial f_{QE}}{\partial m} & 0 & 0 & 0 & 0 & 0 & 0 \\
0 & 0 & 0 & \frac{\partial f_{Qh}}{\partial \tau} & \omega_D+\frac{\partial f_{Qh}}{\partial d} & 0 & 0 & 0 & 0 \\
0 & 0 & 0 & \frac{\partial f_{QE}}{\partial \tau} & \frac{\partial f_{QE}}{\partial d} & \gamma S\omega_D+\frac{\partial f_{QE}}{\partial m} & 0 & 0 & 0 \\
0 & 0 & 0 & 0 & 0 & 0 & \frac{\partial f_{Qh}}{\partial \tau} & \omega_E+\frac{\partial f_{Qh}}{\partial d} & 0 \\
0 & 0 & 0 & 0 & 0 & 0 & \frac{\partial f_{QE}}{\partial \tau} & \frac{\partial f_{QE}}{\partial d} & \gamma S\omega_E+\frac{\partial f_{QE}}{\partial m} \\
1 & 0 & 0 & 1 & 0 & 0 & 1 & 0 & 0 \\
0 & 1 & 0 & 0 & 1 & 0 & 0 & 1 & 0 \\
0 & 0 & 1 & 0 & 0 & 1 & 0 & 0 & 1
\end{pmatrix}
\times \begin{pmatrix} C_\tau \\ C_d \\ C_m \\ D_\tau \\ D_d \\ D_m \\ E_\tau \\ E_d \\ E_m \end{pmatrix} = - \begin{pmatrix} 0 \\ 0 \\ 0 \\ 0 \\ 0 \\ 0 \\ B_\tau \\ B_d \\ B_m \end{pmatrix}. \tag{A.9}$$

(*B*) *Coefficients of the solutions $O(\delta)$ for extreme soil moisture distributions*

B.1. — $G(s)=0$

In the particular case of $G(s)=0$ we have that:

$$f_{QE}=f_{Qh}, \tag{B.1}$$

$$\frac{\partial f_{QE}}{\partial m}=\frac{\partial f_{QE}}{\partial \theta_e}=0. \tag{B.2}$$

Eqs. (A.1) and (A.2) are now independent on m, and form a separate system in the variables τ and d. Taking the same convention as in Appendix A and substituting from (60)–(64) such a system is:

$$\frac{1}{\beta_\chi}\dot{\tau}+\left(1+\frac{\lambda}{\chi}\right)\tau+\alpha d$$
$$=\mu_d\alpha(e^{\sigma t}-1)\mp\frac{2\alpha D}{L}e^{\sigma t} \tag{B.3}$$

$$\frac{1}{\chi}\dot{d}+\alpha d+\tau$$
$$=\mu_d\alpha(e^{\sigma t}-1)\mp\frac{2\alpha D}{L}e^{\sigma t}. \tag{B.4}$$

Expressing again the solution as in eq. (50), it is straightforward to derive:

$$\begin{pmatrix} A_\tau \\ A_d \end{pmatrix} = \begin{pmatrix} 0 \\ \mu_d \end{pmatrix}, \tag{B.5}$$

$$\left[\left(\lambda+\frac{\sigma}{\beta}\right)\left(\frac{\sigma}{\chi}+\alpha\right)+\sigma\right]\begin{pmatrix} B_\tau \\ B_d \end{pmatrix}$$

$$= \begin{pmatrix} \sigma\left(\mp\frac{2\alpha D}{L}+\alpha\mu_d\right) \\ \left(\lambda+\frac{\sigma}{\beta}\right)\left(\mp\frac{2\alpha D}{L}-\frac{\sigma}{\chi}\mu_d\right)-\sigma\mu_d \end{pmatrix}, \tag{B.6}$$

$$\begin{pmatrix} 1 & \frac{\omega_C}{\chi}+\alpha & 0 & 0 \\ 0 & 0 & 1 & \frac{\omega_D}{\chi}+\alpha \\ 1 & 0 & 1 & 0 \\ 0 & 1 & 0 & 1 \end{pmatrix}$$

$$\times \begin{pmatrix} C_\tau \\ C_d \\ D_\tau \\ D_d \end{pmatrix} = -\begin{pmatrix} 0 \\ 0 \\ B_\tau \\ B_d \end{pmatrix}. \tag{B.7}$$

The homogeneous system is now characterized by the two exponents:

$$(\omega_C, \omega_D) = \frac{\chi}{2}\left[\alpha+\beta\left(1+\frac{\lambda}{\chi}\right)\right]$$

$$\times\left\{\pm\left(1-\frac{4\alpha\beta\frac{\lambda}{\chi}}{\left[\alpha+\beta\left(1+\frac{\lambda}{\chi}\right)\right]^2}\right)^{1/2}-1\right\}, \tag{B.8}$$

both with always negative real parts. The equation for m is reduced to:

$$\frac{\gamma S}{\chi}\dot{m}+\tau+\alpha d$$

$$= \mu_d\alpha(e^{\sigma t}-1)\mp\frac{2\alpha D}{L}e^{\sigma t}, \tag{B.9}$$

from where:

$$\begin{pmatrix} \frac{\gamma S\sigma}{\chi} & \frac{\gamma S\sigma}{\chi} & 0 & 0 \\ 0 & 0 & \frac{\gamma S\omega_C}{\chi} & 0 \\ 0 & 0 & 0 & \frac{\gamma S\omega_D}{\chi} \\ 0 & 1 & 1 & 1 \end{pmatrix}\begin{pmatrix} A_m \\ B_m \\ C_m \\ D_m \end{pmatrix}$$

$$= \begin{pmatrix} \mp\frac{2\alpha D}{L}-(B_\tau+\alpha B_d) \\ -(C_\tau+\alpha C_d) \\ -(D_\tau+\alpha D_d) \\ 0 \end{pmatrix}. \tag{B.10}$$

B.2. — G(s) = 1

In the particular case of $G(s) = 1$ we have that:

$$f_{QE} = f_{QE\,\mathrm{pot}},$$

$$\frac{\partial f_{QE}}{\partial d} = \frac{\partial f_{QE}}{\partial \theta} = 0. \tag{B.12}$$

Eqs. (A.1) and (A.3) are now independent on d, and form a separate system in the variables τ and m. Substituting from (60)–(64) such a system is:

$$\frac{1}{\beta\chi\gamma S}\dot{\tau}+\left(\frac{1}{\gamma^2 S}+\frac{\lambda}{\chi\gamma S}\right)\tau+\alpha m$$

$$= \alpha\mu_e(e^{\sigma t}-1)\mp\frac{2\alpha M}{L}e^{\sigma t}, \tag{B.13}$$

$$\frac{1}{\chi}\dot{m}+\alpha m+\frac{1}{\gamma^2 S}\tau$$

$$= \alpha\mu_e(e^{\sigma t}-1)\mp\frac{2\alpha M}{L}e^{\sigma t}. \tag{B.14}$$

Analogously to the previous case, we obtain:

$$\begin{pmatrix} A_\tau \\ A_m \end{pmatrix} = \begin{pmatrix} 0 \\ \mu_e \end{pmatrix}, \tag{B.15}$$

$$\left[\left(\lambda+\frac{\sigma}{\beta}\right)\left(\frac{\sigma}{\chi}+\alpha\right)+\frac{\sigma}{\gamma}\right]\begin{pmatrix}B_\tau\\B_m\end{pmatrix}=\begin{pmatrix}\gamma S\sigma\left(\mp\frac{2\alpha M}{L}+\alpha\mu_e\right)\\\left(\lambda+\frac{\sigma}{\beta}\right)\left(\mp\frac{2\alpha M}{L}-\frac{\sigma}{\chi}\mu_e\right)-\frac{\sigma}{\gamma}\mu_e\end{pmatrix}, \quad \text{(B.16)}$$

$$\begin{pmatrix}\frac{1}{\gamma} & \gamma S\left(\frac{\omega_C}{\chi}+\alpha\right) & 0 & 0\\ 0 & 0 & \frac{1}{\gamma} & \gamma S\left(\frac{\omega_D}{\chi}+\alpha\right)\\ 1 & 0 & 1 & 0\\ 0 & 1 & 0 & 1\end{pmatrix}$$

$$\times\begin{pmatrix}C_\tau\\Cm\\D_\tau\\D_m\end{pmatrix}=-\begin{pmatrix}0\\0\\B_\tau\\B_m\end{pmatrix}, \quad \text{(B.17)}$$

$$(\omega_C,\omega_D)=\frac{\chi}{2}\left[\alpha+\beta\left(\frac{1}{\gamma}+\frac{\lambda}{\chi}\right)\right]\times\left\{\pm\left(1-\frac{4\alpha\beta\frac{\lambda}{\chi}}{\left[\alpha+\beta\left(\frac{1}{\gamma}+\frac{\lambda}{\chi}\right)\right]^2}\right)^{1/2}-1\right\}. \quad \text{(B.18)}$$

The equation for d is reduced to:

$$\frac{1}{\chi}\dot{d}+\alpha d+\tau=-\alpha\mu_d(\mathrm{e}^{\sigma t}-1)\mp\frac{2\alpha D}{L}\mathrm{e}^{\sigma t}, \quad \text{(B.19)}$$

from where:

$$\begin{pmatrix}A_d\\B_d\\C_d\\D_d\end{pmatrix}=\begin{pmatrix}\mu_d\\\left(\mp\frac{2\alpha D}{L}-B_\tau\right)\Big/\left(\frac{\sigma}{\chi}+\alpha\right)\\-C_\tau\Big/\left(\frac{\omega_C}{\chi}+\alpha\right)\\-D_\tau\Big/\left(\frac{\omega_D}{\chi}+\alpha\right)\end{pmatrix}, \quad \text{(B.20)}$$

$$\omega_E=-\alpha\chi, \quad \text{(B.21)}$$

$$E_d=-(B_d+C_d+D_d). \quad \text{(B.22)}$$

REFERENCES

Bras, R. L. 1990. *Hydrology. An introduction to hydrologic science*. Addison-Wesley Publ. Co., Reading (MA), 643 pp.

Castelli, F., Bras, R. L. and Emanuel, K. A. 1993. An analytical approach to the non-linear dynamics of moist frontogenesis. *J. Atmos. Sci.* **50**, 1504–1518.

Chang, Jy-Tai and Wetzel, P. J. 1991. Effects of spatial variations of soil moisture and vegetation on the evolution of a prestorm environment: a numerical case study. *Mon. Wea. Rev.* **119**, 1368–1382.

Charney, J. G. 1947. The dynamics of long waves in a baroclinic westerly current. *J. Meteor.* **4**, 125–162.

Eady, E. T. 1949. Long waves and cyclone waves. *Tellus* **1**, 33–52.

Emanuel, K. A., Fantini, M. and Thorpe, A. J. 1987. Baroclinic instability in an environment of small stability to slantwise moist convection. Part I: Two-dimensional models. *J. Atmos. Sci.* **44**, 1559–1573.

Entekhabi, D., Rodriguez-Iturbe, I. and Bras, R. L. 1992. Variability in large-scale water balance with landsurface-atmosphere interaction. *J. of Climate* **5**, 798–813.

Entekhabi, D. and Rodriguez-Iturbe, I. 1994. Analytical framework for the characterization of the space-time variability of soil moisture. *Adv. Water Resour.* **17**, 25–45.

Fantini, M. 1991. Baroclinic instability and induced air-sea heat exchange. *Tellus* **43A**, 285–294.

Fast, J. D. and McCorcle, M. D. 1991. The effect of heterogeneous soil moisture on a summer baroclinic circulation in the central United States. *Mon. Wea. Rev.* **119**, 2140–2167.

Houze, R. A., Jr. 1981. Structure of atmospheric precipitation systems: a global survey. *Radio Sci.* **19**, 541–576.

Houze, R. A., Jr. and Hobbs, P. V. 1982. Organization and structures of precipitating cloud systems. *Adv. Geophys.* **24**, 225–315.

Hoskins, B. J. and Bretherton, F. P. 1972. Atmospheric frontogenesis models: Mathematical formulation and solution. *J. Atmos. Sci.* **29**, 11–17.

Lowry, W. P. 1959. The falling rate phase of evaporative soil moisture loss: a critical evaluation. *Bull. Amer. Meteor. Soc.* **40**, 605.

Ookouchi, Y., Segal, M., Kessler, R. C. and Pielke, R. A. 1984. Evaluation of soil moisture effects on the generation and modification of mesoscale circulations. *Mon. Wea. Rev.* **112**, 2281–2292.

Peixoto, J. P. and Oort, A. H. 1992. *Physics of climate*. American Institute of Physics, New York (NY), 520 pp.

Rodriguez-Iturbe, I., Entekhabi, D. and Bras, R. L. 1991. Nonlinear dynamics of soil moisture at climate scales. (I). Stochastic analysis. *Water Resour. Res.* **27**, 1899–1906.

Segal, M., Avissar, R., McCumber, M. C. and Pielke, R. A. 1988. Evaluation of vegetation effects on the generation and modification of mesoscale circulations. *J. Atmos. Sci.* **45**, 2268–2291.

Seltzer, M. A., Passarelli, R. E. and Emanuel, K. A. 1985. The possible role of symmetric instability in the formation of precipitation bands. *J. Atmos. Sci.* **42**, 2207–2219.

Van Ulden, A. P. and Holtslag, A. A. M. 1985. Estimation of atmospheric boundary layer parameters for diffusion applications. *J. Clim. Appl. Met.* **24**, 1196–1207.